Author Manuscript

Author Manuscript

Author Manuscript

Author Manuscript

HHS Public Access

Author manuscript

J Control Release. Author manuscript; available in PMC 2021 May 10.

Published in final edited form as:

J Control Release. 2020 May 10; 321: 259–271. doi:10.1016/j.jconrel.2020.01.052.

The Clearance and Biodistribution of Magnetic Composite Nanoparticles in Healthy and Osteoarthritic Rat Knees

Brittany D. Partain[a,1], **Mythreyi Unni**[b,1], **Carlos Rinaldi**[a,b,**], **Kyle D. Allen**[a,*]

[a]J. Crayton Pruitt Family Department of Biomedical Engineering, University of Florida, Gainesville, FL, USA

[b]Department of Chemical Engineering, University of Florida, Gainesville, FL, USA

Abstract

Intra-articular injections are the most direct route for administering osteoarthritis (OA) therapies, yet how drug carriers distribute within the joint remains understudied. To this end, we developed a magnetic composite nanoparticle that can be tracked with fluorescence *in vivo* via an *in vivo* imaging system (IVIS), and quantified *ex vivo* via electron paramagnetic resonance (EPR) spectroscopy. Using this particle, the effects of age and OA pathogenesis on particle clearance and distribution were evaluated in the medial meniscus transection model of OA (5-, 10-, and 15-month old male Lewis rats). At 9 weeks after meniscus transection, composite nanoparticles were injected and joint clearance was assessed via IVIS. At 2 weeks after injection, animals were euthanized and particle distribution was quantified *ex vivo* via EPR spectroscopy. IVIS and EPR spectroscopy data indicate a predominant amount of particles remained in the joint after 14 days. EPR spectroscopy data suggests particles cleared more slowly from OA knees than from the contralateral control, with particles clearing more slowly from 15-month old rats than from 5- and 10-month old rats. This study demonstrates the importance of including both age and OA as factors when evaluating nanoparticles for intra-articular drug delivery.

[*]**Correspondence to:** Kyle D. Allen, Ph.D., Associate Professor, J. Crayton Pruitt Family Department of Biomedical Engineering, University of Florida, 1275 Center Drive, Biomedical Sciences Building, Gainesville, Florida 32611. kyle.allen@bme.ufl.edu.

[**]Correspondence to: Carlos Rinaldi, Ph.D., Dean's Leadership Professor and Chair, Department of Chemical Engineering, Professor, J. Crayton Pruitt Family Department of Biomedical Engineering, J. Crayton Pruitt Family Department of Biomedical Engineering and Department of Chemical Engineering, University of Florida, 1030 Center Drive, Department of Chemical Engineering, Gainesville, Florida 32611, (352) 392-0881. carlos.rinaldi@ufl.edu.

[1] Co-first authors.

Author Contributions

BDP conducted and analyzed cytotoxicity experiments, dye stability experiments, live animal experiments, joint-level inflammatory experiments, and IVIS and EPR spectrometry experiments. MU synthesized and characterized particles, conducted and analyzed colloidal stability experiments, assisted and trained BDP for EPR spectrometry experiments. KDA performed MMT surgeries. All authors contributed to the study design and data interpretation. The manuscript was drafted by BDP, with critical feedback and edits from MU, CR, and KDA. All authors agree with the content and interpretation of the data as presented.

Declarations of interest: none

Publisher's Disclaimer: This is a PDF file of an unedited manuscript that has been accepted for publication. As a service to our customers we are providing this early version of the manuscript. The manuscript will undergo copyediting, typesetting, and review of the resulting proof before it is published in its final form. Please note that during the production process errors may be discovered which could affect the content, and all legal disclaimers that apply to the journal pertain.

Author Manuscript Author Manuscript Author Manuscript Author Manuscript

Keywords

Knee Osteoarthritis; Magnetic Nanoparticle; Electron Paramagnetic Resonance Spectroscopy; Age; Superparamagnetic Iron Oxide

1. Introduction

Osteoarthritis (OA) is a chronic, maladaptive joint disease that affects over 30 million U.S. adults [1]. Knee OA, specifically, accounts for 83% of the total OA burden [2]. Despite ongoing research, no cure for OA exists. Thus, clinical care focuses on palliative treatments to reduce inflammation and treat pain [4]. These palliative treatments include intra-articular injections, which simultaneously increase drug bioavailability and decrease off-target effects. However, the benefits of intra-articular injections are often diminished by rapid drug clearance from the joint [5]. This limitation has spurred research into drug carriers suitable for controlled intra-articular delivery [6].

Recently, significant attention has focused on engineering nanoparticle drug carriers for targeted delivery within the diseased joint. Design parameters, including surface physicochemical properties and the addition of targeting surface ligands, have proven important for controlled drug delivery [6,7]. In this context, nanoparticle characterization, distribution in the joint, and clearance from the joint are important aspects for evaluating potential formulations for clinical translation. However, most characterization of drug or particle clearance has been done using young animals (rats 7–12 weeks old or mice 4–10 weeks old [8–12]), and OA pathophysiology is clearly connected to age [13,14]. Lymphatic function is known to change with age, where aged lymphatic vessels have decreased pumping indices, impaired pathogen clearance, and impaired permeability [15]. Synovial permeability is also altered by age and OA, as diseased and aged synovium is characterized by an increased infiltration of inflammatory cells. The subsequent inflammatory environment leads to altered trans-synovial flow, which changes synovial permeability [16,17]. As such, OA therapeutic studies should consider age as a variable when evaluating nanoparticle and drug distribution and clearance from joints.

Joint clearance and biodistribution have traditionally been assessed using radiolabeled molecule tracking and fluorescence imaging [9,11,12,18–24]. While radiolabeled molecules allow for quantitative measurement of clearance and biodistribution with sensitivities in the picomolar range [25], they have several drawbacks. Isotopes with short half-lives (seconds to hours) are subject to radioactive decay, and therefore methods to track radiolabeled molecules lose their reliability for long term *in vivo* clearance studies. Incorporating radiolabeled molecules into particle systems also requires modification of the particles' surface chemistry, which may cause labeled particles to have different physical properties from unlabeled particles. Furthermore, the synthesis and disposal of radioactive materials is costly and poses potential health hazards. On the other hand, fluorescence imaging, by either conjugating or loading particles with fluorescent dyes, provides a noninvasive method to track agents longitudinally with high sensitivity and temporal resolution [26]. However, *in vivo* fluorescence imaging is subject to light scattering, signal attenuation, and

Author Manuscript Author Manuscript Author Manuscript Author Manuscript

autofluorescence. Additionally, dye release from particle carriers may make it difficult to distinguish between signal from loaded dye or free dye. Implementing near-infrared (NIR) dyes in particle carriers mitigates but does not completely resolve these limitations. NIR dyes avoid the excitation and emission range associated with tissue autofluorescence, and have increased tissue penetration depth because their excitation and emission ranges do not overlap with those of hemoglobin absorption [10,26]. However, light scattering and signal attenuation from tissue is inevitable and heterogeneous, ultimately limiting the ability of *in vivo* fluorescence imaging to quantitatively track organ and joint tissue biodistribution.

While fluorescence imaging with NIR dyes can help evaluate particle clearance, understanding where particles distribute within the joint and within the body is also important. Superparamagnetic nanoparticles can be accurately and selectively quantified with electron paramagnetic resonance (EPR) spectroscopy [27,28]. EPR spectroscopy measures the paramagnetic properties of iron oxide nanoparticles. Specifically, the unpaired electron spins in paramagnetic materials can split into two opposing energy states. Upon increasing the magnetic field, the energy difference of the split states increases. The energy difference can be tuned to equal an external microwave frequency, allowing for transitions between spin states. The net energy absorbed during transitions is recorded as a spectral line per spin transition. The area under the first derivative of the absorption spectra is related to the electron's magnetic moments, and thereby to the concentration of iron oxide nanoparticles in a tissue sample [29,30].

To address some of the challenges in evaluating nanoparticle biodistribution and clearance from the joint, we developed a magnetic composite nanoparticle platform, termed composite nanoparticles, to quantify particle clearance and biodistribution in healthy and osteoarthritic rat knees via fluorescent particle imaging and EPR spectroscopy. First polyethylene glycol coated composite nanoparticles containing NIR dye and superparamagnetic iron oxide nanoparticles were synthesized and thoroughly characterized. Then, the unique aspects of our composite nanoparticles were exploited to quantitatively assess how age and OA affect nanoparticle clearance and biodistribution in joint tissues and throughout the body of male Lewis rats.

2. Materials and Methods

2.1. Magnetic Nanoparticle Synthesis and Composite Nanoparticle Formulation

2.1.1 Oleic Acid Coated Iron Oxide Nanoparticle Synthesis—Oleic acid coated iron oxide nanoparticles were synthesized via semi-batch thermal decomposition in the presence of molecular oxygen [31]. First, an iron oleate precursor was synthesized by reacting iron acetylacetonate (>98% pure, TCI America, Portland, OR, USA) and oleic acid (90% technical grade, Sigma-Aldrich, St. Louis, MO, USA) at 320°C under argon (Ar) atmosphere (Airgas, Gainesville, FL, USA). A mixture of iron oleate and octadecene (90% technical grade, Sigma-Aldrich, St. Louis, MO, USA) was added at 9 mL/h into docosane (90% pure, Sigma-Aldrich, St. Louis, MO, USA) at 350 °C for eight hours. The synthesis was performed with oxygen feed of 20% oxygen and 80% Ar (Airgas, Gainesville, FL, USA) at a rate of 9.47 sccm and controlled using a mass flow controller (Bronkhorst USA, Bethlehem, PA, USA). Additional Ar gas was introduced into the reactor head space to

Author Manuscript Author Manuscript Author Manuscript Author Manuscript

maintain the overall oxygen concentration below 5% and avoid flashing of the organic vapor. The unreacted reagents were washed by solvent - antisolvent precipitation where the product was initially suspended in chloroform (Sigma-Aldrich, St. Louis, MO, USA) and then precipitated with acetone (Fisher Scientific, Hampton, NH, USA) in a 1:2 volume ratio till oleic acid coated particles with 60 wt% iron were obtained.

2.1.2 Composite Nanoparticle Formulation—Flash nanoprecipitation was employed to produce the composite nanoparticles containing magnetic nanoparticles and NIR dye [32]. Briefly, oleic acid coated iron oxide nanoparticles, $PEG_{4.9kDa}$-b-$PLA_{6.0kDa}$ (Evonik Industries, Essen, Germany), and the near IR lipophilic tracer 1,1'-Dioctadecyl-3,3,3',3'-tetramethylindotricarbocyanine iodide (DiR) (Marker Gene Technologies, Inc. Eugene, OR, USA) were suspended in tetrahydrofuran (THF) (inhibitor free, HPLC grade, >99%, Sigma-Aldrich, St. Louis, MO, USA) and used as an inlet stream. The relative mass fractions of these soluble components were 58% iron, 36% block copolymer, and 6% DiR. The solutes in this inlet stream were rapidly mixed against equal volumes of a miscible antisolvent (DI water) in a confined impinging jet mixer (Fig. 1). Mixing of streams was conducted using a syringe pump at 52 mL/min (KD Scientific Inc.,Holliston, MA, USA), and the resulting particles were precipitated into a water reservoir. The precipitated composite nanoparticles were washed using a magnetic separation column (Miltenyi Biotec, Bergisch Gladbach, Germany) to remove free polymer and unencapsulated DiR. The particles were washed with water at least four times or until the filtrate was free of fluorescent DiR signal. The particles were recovered by removing the magnetic column from the magnet and flushing with DI water. The final particle stock was stored at 4 °C.

2.2. Composite Nanoparticle Characterization

2.2.1 Physical Diameter—Composite nanoparticles were imaged using a Hitachi H 7000 transmission electron microscope. Composite nanoparticles in water were sampled on ultrathin nickel type B grids coated with 3–4 nm carbon and 5–6 nm Formvar (Electron Microscopy Sciences, Hatfield, PA, USA). Images of particles were acquired using a Veleta CCD side-mount camera, and the physical diameter and size distribution were analyzed using ImageJ [33].

2.2.2 Hydrodynamic Diameter and Surface Charge—The composite nanoparticle hydrodynamic diameter and size distribution was evaluated by dynamic light scattering (DLS), and composite nanoparticle surface charge was evaluated by zeta potential measurement, using a particle analyzer (Zeta PALS, Brookhaven Instruments, Holtsville, NY, USA) with ~633 nm laser excitation. For the zeta potential measurements, the nanoparticle stock solutions were prepared in water and diluted to ~1% v/v with adjusted ionic strength using 1 mM KNO_3 (Fisher Scientific, Hampton, NH, USA) at pH 7.4.

2.2.3 Magnetic Properties—Magnetic properties of the synthesized composite nanoparticles were evaluated using a magnetic property measurement system (MPMS 3, Quantum Design, San Diego, CA) with a superconducting quantum inference device (SQUID) magnetometer. Measurements were made at 300 K in a magnetic field range from 7 T to −7 T. The saturation magnetization of composite nanoparticle was deduced from the

Author Manuscript Author Manuscript Author Manuscript Author Manuscript

maximum of the magnetization obtained from the magnetization curve. The volume-weighted median magnetic diameter (D_{mv}) and geometric deviation of oleic acid coated magnetic nanoparticle samples were determined by fitting the superparamagnetic equilibrium magnetization curve to the Langevin function weighted by a lognormal size distribution [34].

2.2.4 Iron Quantification—The *o*-phenanthroline assay was performed to quantify the amount of iron in the composite nanoparticles. Composite nanoparticles, suspended in water, were digested in 70% concentrated HNO_3 (optima grade, Fisher Scientific, Hampton, NH, USA) and left overnight at 101 °C in a dry heating block. The next day, 50 μL of digested sample were dried at 115 °C. 46 μL of water were added to vials containing particles in THF and particles in water. Iron was further reduced with hydroxylamine hydrochloride (30 μL, 8.06 M) (Sigma-Aldrich, St. Louis, MO, USA) for 1 hour. Next, 1,10-phenanthroline monohydrate (75 μL, 13 mM) (Sigma-Aldrich, St. Louis, MO, USA) was added to complex with Fe^{2+}, then promoted using sodium acetate (49 μL, 1.22 M) (Sigma-Aldrich, St. Louis, MO, USA). The absorbance of samples (100 μL) was measured at 508 nm in a SpectraMax M5 microplate reader (Molecular Devices, San Jose, CA, USA). Running each sample in triplicate, concentrations were determined from a standard curve prepared from an iron standard solution (Fluka iron standard for ICP).

2.3. In Vitro *Characterization*

2.3.1 Fluorescent Dye Retention in Composite Nanoparticles—Dye retention within the composite nanoparticles was determined by quantifying DiR remaining over 14 days. To mimic physiological conditions, composite nanoparticles were suspended in bovine synovial fluid (1.6 mg iron oxide/mL) and maintained at 37 °C in a shaker at 50 rpm. Samples were removed immediately after being suspended in synovial fluid and after incubating for 1, 3, 5, 7, 10, and 14 days (n = 3 per time point). At each time point, composite nanoparticles were magnetically separated from the free dye, and the synovial fluid was removed from each tube. Composite nanoparticles were resuspended in THF and vortexed to release the remaining dye. Then, the solutions were separated again using a magnetic column, and the dye/THF solution imaged in a black 96 well plate using IVIS (PerkinElmer, Waltham, MA, USA). Fluorescence intensity was measured at an excitation of 745 nm and emission of 840 nm.

An additional two-day study was conducted to demonstrate dye association with composite nanoparticles. Methods and results can be found in the supplemental information (Supplemental Fig. S1).

2.3.2 Cobalt Ferrite Composite Nanoparticle Colloidal Stability—Dynamic magnetic susceptibility (DMS) measurements were used to evaluate particle colloidal stability in bovine synovial fluid over 14 days. $PEG_{4.9kDa}$-b-$PLA_{6.0kDa}$ coated cobalt ferrite composite particles, prepared using flash nanoprecipitation, were used for this study. Particle stability was assessed immediately after addition to synovial fluid and after incubating for 1, 3, 5, 9, 12, and 14 days. DMS measurements were performed using a commercial AC susceptometer (Dynomag system, Acreo Swedish ICT) at room temperature. The amplitude

Author Manuscript Author Manuscript Author Manuscript Author Manuscript

of the excitation field varied between 0 and 0.5 mT, and the frequency interval was evaluated in a range of 10 Hz to 160 kHz. All DMS measurements were fit to the Debye model of dynamic susceptibility [35,36] with two assumptions. First, the particles were assumed to have a log-normal size distribution. Second, the infinite shear viscosity was assumed to be that of bovine synovial fluid. Rheological measurements of bovine synovial fluid were performed using an Anton Parr MCR 702 twin drive rheometer.

2.3.3 Composite Nanoparticle Cytotoxicity—To assess composite nanoparticle cytotoxicity, synoviocyte proliferation was evaluated via MTS CellTiter 96 Aqueous Proliferation Assay (Promega, Madison, WI, USA). Briefly, primary rat synoviocytes were isolated from the synovium surrounding the medial and lateral sides of the femoral chondyle. The synovium was digested in a 0.2% collagenase I solution (Worthington Biochemical Corporation, Lakewood, NJ, USA) for 24 hours at 37 °C and shaking at 40 rpm. After 24 hours the synovium was completely digested, and cells were passed through a cell strainer, centrifuged, and resuspended in fresh media. Then, rat synoviocytes (3000 passage 1 cells/well in 96 well plate) were cultured in media for 24 hours and incubated at 37 °C under 5% carbon dioxide. Then, cells were cultured in media containing varying nanoparticle concentrations (0, 0.01, 0.05, 0.1, 0.5, 1.0, 1.5, and 2.0 mg iron oxide/mL) for 24 hours. Nanoparticle media suspensions were removed, and cells were washed to remove remaining particles. Cells were cultured for 48 hours, after which media was replaced with fresh media and MTS assay reagents. After two hours, media with MTS assay reagent was stirred, removed, and magnetically separated to ensure all particles were removed. Absorbance was measured at 490 nm on a microplate reader (BioTek Synergy 2, Winooski, VT, USA).

To further evaluate composite nanoparticle cytotoxicity, cartilage explants were exposed to particles. Cartilage explants (4 mm) were aseptically collected from the femoral condyles of a juvenile male bovine (Research 87 Inc., Boylston, MA, USA). Immediately after collection, explants were plated in a petri dish and washed with media containing 1% penicillin-streptomycin. Then, explants were incubated at 37 °C and 5% carbon dioxide for 24 hours. Next, cartilage biopsies were plated in 96 well plates with the articular surface facing up. Explants were then incubated with varying nanoparticle concentrations as described above. After 24 hours, nanoparticle media suspensions were removed and explants were washed to remove remaining particles. Each well was replenished with fresh media and incubated for 48 hours. After that time, media was replaced with fresh media and MTS assay reagent. After an hour and a half, media with MTS assay reagent was stirred, removed, magnetically separated, and plated in duplicate for measurement on a plate reader. Explants were dabbed-dry and weighed. Data were normalized on the basis of weight.

2.4. *Experimental Design for* In Vivo *Evaluation of Composite Nanoparticle Joint Clearance*

In vivo joint clearance and distribution were measured and compared in healthy and OA joints from male Lewis rats (5-, 10-, and 15-months at the time of injection, Charles River Laboratories, Wilmington, MA, USA). To induce OA, surgical transection of both the medial collateral ligament (MCL) and medial meniscus were performed in all rats [5-months

Author Manuscript Author Manuscript Author Manuscript Author Manuscript

(n = 12), 10-months (n = 12), and 15-months (n = 8)]. One 5-month old rat and one 15-month rat were lost due to surgical complication resulting in n = 11 for both groups. After 9 weeks, 8 rats from each age group received composite nanoparticle injections to their OA and contralateral joints. Remaining rats (n = 3 for the 5- and 15-month and n = 4 for the 10-month groups) were used as age matched controls for background fluorescence signal and EPR spectra. IVIS measurements were acquired at an excitation of 745 nm and an emission of 840 nm. Rats were imaged at the following time points: before injection; immediately after injection; at 5, 10, 15, 30 minutes after injection; at 1, 2, 4, 8, 12 hours after injection; and daily from 1 to 14 days after injection. At 14 days post-injection, rats were euthanized via exsanguination under deep anesthesia. Organs and joint tissues were collected for endpoint IVIS imaging and EPR spectroscopy analysis. All live animal procedures were approved by the University of Florida's Institutional Animal Care and Use Committee.

2.4.1 Medial Collateral Ligament Transection (MCLT) and Medial Meniscus Transection (MMT) Surgery

Rats were anesthetized in a 3% isoflurane sleep box (Patterson Veterinary, Greenley, CO, USA), aseptically prepped with alternating betadine surgical scrub (Purdue Products, Stamford, CT, USA) and 70% isopropyl alcohol in triplicate, and transferred to a sterile field. During MCLT and MMT surgery, a 1–2 cm midline skin incision was made along the medial side of the knee. Skin was retracted and the MCL was exposed by blunt dissection, and transected. The knee was moved into a valgus orientation, allowing central aspects of the medial meniscus to be cut radially. After meniscus transection, absorbable 5–0 vicryl braided sutures (Ethicon, Somerville, NJ, USA) were used to internally close the surgical path; 4–0 ethilon nylon monofilament sutures (Ethicon, Somerville, NJ, USA) were used to close the skin. Anesthesia was maintained via mask inhalation of 2.5% isoflurane throughout all procedures. Rats recovered post-operatively in a warming box until ambulatory. For pain management, rats received buprenorphine (0.05 mg/kg) (Patterson Veterinary, Greeley, CO, USA) subcutaneously every 12 hours for 48 hours post-surgery.

2.4.2 Composite Nanoparticle Injection

At 9 weeks after OA induction, rats (n = 8 per age) were anesthetized using 2.5% isoflurane, and the injection site was aseptically prepped, as described previously. While under anesthesia, composite nanoparticles suspended in 25 μL sterile saline were injected in both knees using a 0.3 mL insulin syringe (29G × 1/2'") (Smiths Medical ASD Inc., Keene, NH, USA). The injection concentration of composite nanoparticles was 2.65 mg iron oxide/mL. The final concentration of composite nanoparticles in the joint was estimated to be 1.6 mg iron oxide/mL (assuming there is 50 μL of synovial fluid in the joint). For injections, the needle was inserted through the patellar ligament, following the patellar groove to the central aspects of the knee. After the injection, the knee was flexed 10 times to mix the particle solution and synovial fluid, and the injection site was cleaned with sterile gauze and 70% ethanol.

2.4.3 In Vivo *Composite Nanoparticle Clearance from OA and Contralateral Knees*—

Rats were imaged (as described above) for 14 days after injection using IVIS. For assessment, a region of interest (ROI) was drawn around the largest signal, with an

Author Manuscript Author Manuscript Author Manuscript Author Manuscript

identically sized ROI for all knees. Non-injected animals were imaged and used for background subtraction. All data were normalized by individual rat to its day 0 radiant efficiency value. We chose to present clearance in relative terms because this measure was used by other intra-articular clearance studies to show differences relative to the day 0 radiant efficiency value [9,12,37].

2.5. Joint-Level Inflammatory Response

After euthanasia, the patella tendon was cut above the patella and reflected down. Synovial fluid was extracted from the joint using fluid wicking [38]. Briefly, a 4 mm diameter alginate sponge (Melgisorb, Göteborg, Sweden) was inserted into the joint, and the knee was flexed ten times. After absorbing synovial fluid, the alginate sponge was removed and placed in alginate lyase (35 μL, 1-unit/mL) (Sigma-Aldrich, St. Louis, MO, USA). All samples were briefly vortexed, then placed in a 34 °C water bath for 30 minutes. Sodium citrate (15 μL, 1.0 M) (Sigma-Aldrich, St. Louis, MO, USA) was added to each sample. The volume of the sample was then determined using the pipette-dialing method.

Protein levels of IL-1β, IL-6, IFN-γ, and TNF-α were quantified via a pro-inflammatory multiplex immunoassay, according to manufacturer specifications (Meso Scale Diagnostics, Rockville, MD, USA). Data were normalized by sample volume.

2.6. Ex Vivo *Determination of Composite Nanoparticle Joint Clearance and Biodistribution*

After synovial fluid wicking, joint tissues including the femur, patellar synovium/fat pad, tibia, and menisci were isolated for joint distribution analysis. Samples from the femur included the femoral cartilage and synovium from the suprapatellar bursa. Samples from the patella included the patellar cartilage and synovium, as well as the fat pad and prepatellar and infrapatellar bursa. Samples from the tibia included the tibial cartilage and synovium. The heart, liver, spleen, kidneys, bladder, lungs, popliteal lymph nodes, and inguinal lymph nodes were also isolated for biodistribution analysis. All organs, joint tissues, and lymph nodes were imaged using IVIS with the same parameters as with live rats. Non-injected animals' organs and joint tissues were used for background fluorescence subtraction.

2.6.1 Electron Paramagnetic Resonance (EPR) Spectroscopy Measurements

—Immediately after IVIS imaging, vital organs, joint tissues, and lymph nodes were weighed and lyophilized for 5 days or until dry. Then, vital organs, joint tissues, and lymph nodes were weighed again (dry weight) and crushed. A mass of 25–30 mg from each vital organ was placed in gelatin capsules in triplicate, while individual joint tissues and lymph nodes were loaded into one gelatin capsule each. EPR (Bruker ELEXSYS-II E500 at 9.83 GHz and field sweep of −6000 to 6000 Gauss) was utilized to quantify the amount of magnetite (Fe_3O_4) in each sample. Samples were normalized by whole organ weight. Non-injected animals' organs and joint tissues were used for background iron subtraction.

2.7 Statistical Analysis

All statistical tests, described below, were performed using Statistica (Palo Alto, CA, USA). A $p<0.05$ was used for statistical significance.

Author Manuscript Author Manuscript Author Manuscript Author Manuscript

2.7.1 In Vitro *Composite Nanoparticle Cytotoxicity*—1-sample Student's t-tests were used to detect if synoviocyte and cartilage explant viability was less than 100% viability at each nanoparticle concentration. Since the null hypothesis aligns with the desired outcome (no cytotoxicity), we did not correct for compounding type 1 error.

2.7.2 In Vivo *Clearance from OA and Contralateral Knees*—Paired Student's t-test were used to detect clearance differences in OA and contralateral joints for each age group (area under curve analysis).

2.7.3 Joint-Level Inflammatory Response—Joint-level inflammatory responses for protein levels of IL-1β, IL-6, IFN-γ, and TNF-α were assessed by unpaired Student's t-tests for contralateral and OA knees. Again, since the null hypothesis aligned with the desired outcome (no inflammatory response), we did not correct for compounding type 1 error. This study was designed to detect a foreign body response to composite nanoparticles, not OA related changes.

2.7.4 Ex Vivo *Biodistribution*—A one-way ANOVA followed by Tukey's HSD *post hoc* was used to compare % total iron oxide remaining in the body and each vital organ, as a function of age. Differences between particle distribution in OA and contralateral joints and joint tissues as a function of age were determined by a two-way ANOVA followed by Tukey's HSD post hoc. Reported p values were determined via Tukey's HSD post hoc, or otherwise specified as an ANOVA main effect.

3. Results

3.1 *Composite nanoparticles were characterized and determined to be colloidally stable and retain DiR dye in synovial fluid* ex vivo

TEM shows representative particle morphology for our composite nanoparticles (Fig. 2A). Furthermore, composite nanoparticles had a hydrodynamic diameter of 195 nm ± 39 nm (Fig. 2B), a zeta potential of −17 mV, and were superparamagnetic with a saturation magnetization of 85.88 Am^2/kg corresponding to magnetite (Fig. 2C). Evaluation of DiR retention in composite nanoparticles *in vitro* showed that 36% of total dye remained after 14 days (Fig. 2D). Furthermore, dye association with composite nanoparticles can be visualized after 2 days (Supplemental Fig. S1). DMS measurements suggest that hydrodynamic diameters of the composite nanoparticles did not change significantly while incubating in synovial fluid over 14 days (Supplemental Fig. S2).

3.2 *Composite nanoparticles are not cytotoxic to synoviocytes or cartilage explants* ex vivo

Both synoviocytes and cartilage explants remained viable at all concentrations tested (Supplemental Fig. S3). However, at a concentration of 2.0 mg iron oxide/mL, synoviocyte % viability began to drop, with a difference relative to 100% nearing significant ($p = 0.08$). Although this trend was observed, the concentration subsequently used *in vivo* (1.6 mg iron oxide/mL) did not have cytotoxic effects *in vitro*.

Author Manuscript Author Manuscript Author Manuscript Author Manuscript

3.3 While particles clear from joints, IVIS detected that many particles remain in OA and contralateral joints at 14 days

IVIS images show fluorescence signal in both the OA and contralateral knees at 14 days for all rats (Fig. 3). Using IVIS radiant efficiency signal, area under the curve (AUC) analysis was utilized to evaluate clearance for 14 days after injection. In 5-month ($p = 0.2$) and 15-month old rats ($p = 0.8$), particle clearance was not significantly different for OA and contralateral joints. Whereas in 10-month old rats, particles cleared faster from the OA joint ($p = 0.03$) (Fig. 4). After 14 days, fluorescence signal remained above the limit of detection for all rats, suggesting that NIR dye remained in the joints. Furthermore, at the day 14 time point, there were no differences between OA and contralateral fluorescence signals for all rats.

3.4 Composite nanoparticles do not elicit a joint-level inflammatory response

After 14 days of particle exposure, protein levels of IL-1β in the joint were below the limit of detection for most samples. Recall, this study was designed to detect a foreign body response to composite nanoparticles, not OA related changes. There were no differences between protein levels in the OA injected and OA non-injected knees for IL-6 ($p = 0.8$), IFN-γ ($p = 0.3$), and TNF-α ($p = 0.8$). Additionally, there were no differences between protein levels in the contralateral injected and contralateral non-injected knees for IL-6 ($p = 0.8$), IFN-γ ($p = 0.5$), and TNF-α ($p = 0.2$) (Supplemental Table S1).

3.5 IVIS and EPR spectroscopy are complementary techniques that show higher composite nanoparticle retention in both knees compared to other organs

For particle biodistribution in all ages, both IVIS and EPR (Fig. 5) showed higher particle presence in the knees at 14 days post-injection compared to other organs. Only one rat in the 5-month old group showed high liver signal determined by both IVIS and EPR. IVIS fluorescence signal was not detected in the liver for the 10-month and 15-month groups; however, EPR quantified 4.4% and 4.9% of the total iron particles injected remained in the liver of the 10-month and 15-month animals, respectively.

3.6 EPR spectroscopy can selectively quantify composite nanoparticle distribution changes associated with OA and age in the vital organs and knees

Although IVIS and EPR consistently showed greatest particle retention in both OA and contralateral knees compared to other organs, IVIS and EPR showed different particle distribution patterns in specific joint tissues (Fig. 6). For 5- and 10-month animals, IVIS indicated greatest signal intensity in the meniscus, while EPR indicated the least iron oxide accumulation in the meniscus. EPR spectroscopy's high selectivity and sensitivity (lower limit of detection = 0.066 μg iron) was used to tease out distribution changes associated with age and disease. After 14 days, the aggregate sum of vital organs and knees quantified 44.7% of composite nanoparticles remained in 5-month animals, 45.1% in 10-month animals, and 62.5% in 15-month animals (Fig. 7A). Significantly more nanoparticles remained in the vital organs and knees of 15-month animals compared to the 5-month ($p = 0.0002$) and 10-month ($p = 0.0002$) animals.

Author Manuscript Author Manuscript Author Manuscript Author Manuscript

EPR spectroscopy detected nanoparticles in the heart (Fig. 7B), lungs (Fig. 7C), spleen (Fig. 7D), kidneys (Fig. 7E), and liver (Fig. 7F). Most of the bladder samples had signals below the limit of detection. As a function of age, the distribution of composite nanoparticles was similar in vital organs (Fig. 7). However, nanoparticle distribution in OA and contralateral knees ($p = 0.02$ ANOVA, main effect) was significantly different, with more nanoparticles remaining in the OA knee after 14 days for all animals at all ages (Fig. 8A). 5-month animals retained 19.4% and 15.9% of the nanoparticles in their OA and contralateral knees, respectively. 10-month animals retained 17.9% and 16.0 % of the nanoparticles in their OA and contralateral knees respectively. 15-month animals retained 24.1% and 21.2% of the nanoparticles in their OA and contralateral knees, respectively. Furthermore, the 15-month animals had significantly more nanoparticles in their knees than the 5-month ($p = 0.002$) and 10-month ($p = 0.0004$) animals. All but three lymph node samples were below the limit of detection (Supplemental Fig. S4).

Tissue regions of OA and contralateral knees were dissected to further quantify where nanoparticles distributed within the joint. Most of the nanoparticles distributed to the patella/fat pad region (Fig. 8B), followed by the femoral tissue region (Fig. 8C), the tibial tissue region (Fig. 8D), and lastly the menisci (Fig. 8E). Age was a significant factor for nanoparticle accumulation in the patella/fat pad region ($p = 0.04$, ANOVA, main effect), whereas disease played a significant role in nanoparticle accumulation in the femoral tissue and menisci. More nanoparticles were retained in the femoral tissue of the OA knee ($p = 0.002$), while more nanoparticles were retained in the menisci of the contralateral knee ($p = 0.04$).

Finally, nanoparticle accumulation in lymph nodes was negligible after 14 days, with only three samples above the lower limit of detection. All three detectable samples were from the contralateral lymph nodes of 5-month old animals (Supplemental Fig. S4).

4. Discussion

Understanding joint clearance and distribution is vital to develop better retention strategies for intra-articular OA therapeutics. In prior work, clearance from the joint has been characterized for nanomaterials specifically developed to improve whole-joint retention [9,12,37,39–45]. Studies have evaluated how particle size affects intra-articular clearance from healthy and diseased knees [11,46]. However, physiological variables, like age and disease, have not been thoroughly investigated for effects on nanoparticle clearance. To this end, this study evaluated nanoparticle clearance and biodistribution differences in male Lewis rats as a function of age and OA using IVIS and EPR spectroscopy.

To evaluate nanoparticle clearance and biodistribution, a multimodal composite nanoparticle was developed, wherein a NIR dye was imaged via fluorescence and the magnetic particle component was quantified via EPR spectroscopy. Using this particle, IVIS was employed to evaluate *in vivo* biodistribution semi-quantitatively, and EPR spectroscopy to quantify superparamagnetic iron oxide content in samples. EPR spectroscopy has been used in other models, primarily cancer, to selectively and quantitatively measure how iron oxide nanoparticle biodistribution is altered in physiological systems [27,29,47]. In this first

Author Manuscript Author Manuscript Author Manuscript Author Manuscript

application of EPR spectroscopy to intra-articular biodistribution, EPR data demonstrates how this quantitative technique can be beneficial in understanding the physiology of joint clearance. Moreover, the high sensitivity of EPR spectroscopy is a complement to IVIS data, detecting nuances of nanoparticle clearance associated with age and OA.

EPR and IVIS data indicated a predominant amount of particles remained in the joint after 14 days; however, only EPR detected a measurable amount of iron oxide in the liver. In IVIS data, the minimal liver load could be attributed to high fluorescence signal attenuation by liver tissues. Additionally, these particle distribution differences could be attributed to light scattering, tissue autofluorescence, the semi-quantitative nature of IVIS, and the fact that light penetration depth into tissues is only a few millimeters [26]. EPR spectroscopy is not affected by the aforementioned issues and could sensitively quantify nanoparticle accumulation in the liver. In EPR data, minimal nanoparticle accumulation was shown in the liver of 5-month old rats (with the exception of one rat), whereas roughly 5% of remaining nanoparticles were retained in 10-month and 15-month rat livers. Changes in liver accumulation with age were not anticipated, and it is not known why more composite nanoparticles are retained in older rat livers following intra-articular injection. However, previous studies have demonstrated that increased age is associated with pharmacokinetic changes, including reduced clearance by the liver [48]. As such, age-related impairment of liver metabolism [49] may account for increased particle retention in 10- and 15-month rat livers, as well as significantly more particles in 15-month rats. In addition, EPR spectroscopy results demonstrate significantly more particles were retained in 15-month rat knees, indicating age plays an important role in nanoparticle retention in the knees.

In addition to age, disease also plays an important role in nanoparticle retention and distribution in the knee. Previous work by Mwangi et al. [46] demonstrated the clearance of 500 kDa dextran molecules decreased in MMT joints compared to un-operated joints, which was possibly attributed to synovial thickening. Doan et al. [50] explored how increased endothelin-1, a vasoconstrictor found in OA synovial fluid, impaired 40 kDa PEG clearance from the articular joint. Although the molecules in the aforementioned studies were smaller and less rigid than our composite nanoparticle, their findings suggest disease impairs joint clearance.

While our EPR data aligns with these prior studies, our IVIS clearance data differed. In our longitudinal IVIS data, more particles tended to be retained in the contralateral joint for the 5-month old rats (non-significant), and were significantly higher in the contralateral knee of 10-month old rats. However, no differences were found between OA and contralateral joints for 15-month rats. Lack of differences between 15-month rat knees could be associated with the development of age-related OA in both knees of these animals. Particle and dye stability could account for the inconsistency between IVIS and EPR data. After 14 days, 36% of the total dye remained in the particles, yet particle hydrodynamic diameter did not change. These results suggest iron oxide nanoparticles remained in composite nanoparticles, while the fluorescent dye was slowly released. Both encapsulated dye and free dye interacting with tissue compartments could be contributing to the fluorescence signal reported in IVIS data. Furthermore, longitudinal IVIS data shows fluorescence signal increases and peaks two to three days after injection. This trend is not unique to our methodology and has been

Author Manuscript Author Manuscript Author Manuscript Author Manuscript

observed in other intra-articular delivery papers [1 2]. In fact, Kim et al. observed an increase in fluorescence following intra-articular injection of the same dye, yet the causes of this phenomenon have not been explained [12,37].

On the other hand, our EPR spectroscopy data shows higher composite nanoparticle accumulation in the OA joint compared to the contralateral joint for all three age groups, which may occur due to iron oxide nanoparticles being retained in the composite nanoparticles while dye is released. Moreover, EPR results align well with work from Mwangi et al and Doan et al, where nanoparticle clearance is impaired in the diseased joint.

In addition to whole joint clearance, the distribution of particles in joint tissues was affected by disease. Specifically, EPR results suggest OA affected nanoparticle distribution in the menisci and femoral tissue. Although nanoparticle accumulation was minimal in the menisci, there were still significant differences between OA and contralateral joint tissues. This phenomenon could be an artifact of the MMT surgery. By transecting the medial meniscus, we reduced the amount of intact tissues, thus decreasing the medial meniscus mass at 9 weeks after MMT surgery. Alternatively, differences may be attributed to altered mechanical stretching and contracting of menisci during motion, which would affect convective fluid transport into both the medial and lateral meniscus. This loss in convective fluid transport in the OA knee's medial meniscus could account for more particles accumulating in the contralateral knee, where both menisci are intact.

A large amount of particles remaining in the OA and contralateral joints distributed to the femoral tissue. Based on visual observation during dissections, the greatest particle accumulation in the femoral tissue was near the suprapatellar bursa for both OA and contralateral knees. High nanoparticle accumulation in the suprapatellar bursa could be attributed to its anatomical location and lymphatic flow. The suprapatellar bursa is proximal to the knee cap; therefore, upward lymphatic flow may contribute to particle accumulation in this location [51]. Furthermore, EPR data for the femoral region showed higher particle concentration in the OA tissue. Higher particle accumulation in the OA femoral tissue could be attributed to the decrease in mature lymphatic vessels and capillaries found in osteoarthritic knees [52].

Our results could also suggest a breakdown of lymphatic functionality associated with OA. This theory is based upon total nanoparticle accumulation in the OA and contralateral knees, as well as femoral tissue nanoparticle distribution. Lymph nodes were collected and assessed in an attempt to test this theory. All but three lymph nodes were below the limit of detection. Using EPR to quantify particle accumulation in the lymph nodes at earlier time points may have allowed for sufficient composite nanoparticle concentrations for analysis.

How particles clear from the joint is affected by particle size, where smaller particles are more likely to clear through capillary beds and larger particles are more likely to clear through the lymphatics [5]. Several intra-articular delivery studies have evaluated how size affects joint retention [11,46,53]. In this study, one composite nanoparticle size was designed based on suitable magnetic properties for EPR spectroscopy. Specifically, the size and contents of the composite nanoparticle's magnetic core was selected based on the

Author Manuscript Author Manuscript Author Manuscript Author Manuscript

sensitivity of the EPR spectrometer. This was motivated by the study's focus on understanding the effects of physiologic variables on joint clearance, rather than the effects of particle size and physicochemical properties. However, the method used to formulate the composite nanoparticles in this study can be applied to generate particles with a wide range of sizes and surface charge/chemistry, as well as incorporate hydrophobic drugs [32,54].

While this study does not incorporate therapeutics, techniques to track where particles transport can be applied in drug delivery studies. Superparamagnetic iron oxide has been detected via EPR with a sensitivity as low as 5.6 ± 0.8 nmol Fe/g tissue and in the nM range, which is beneficial for drug delivery studies [27,55]. Superparamagnetic iron oxide particles can be and have been incorporated into different systems, including magnetoliposomes, for drug delivery purposes [56–58]. Co-incorporated iron oxide nanoparticles remain superparamagnetic in nature, thereby retaining their ability to be detected via EPR spectroscopy.

EPR spectroscopy can be used as a complementary tool to assess the efficacy of tissue targeting strategies for drug delivery. Specifically, some controversy exists around how nanoparticle size affects penetration into cartilage. One group showed 96 nm nanoparticles cannot pass through the cartilage matrix [59], while others found nanoparticles greater than 100 nm can distribute through cartilage [9,60]. EPR may be a useful technique to explore how magnetic nanoparticle design parameters affect cartilage penetration and tissue targeting as a whole.

Tracking particle retention in the joint is commonly conducted using fluorophores that have been tethered [9,37,53,61] or loaded within the particles [11,12,23]. However, a limitation of this study and others in the field is the reliability of the fluorophore remaining with the particles. Studies conducted solely using a fluorophore to track intra-articular particle clearance and biodistribution may be interpreting data that is actually the distribution of released dye. Although this is a limitation of the study, combining these techniques can be beneficial for future drug delivery studies. IVIS measures fluorescence intensity and EPR quantifies the unpaired electron in iron oxide; therefore, it may be possible to use iron oxide particles loaded with a fluorescently labeled drug to track where the drug distributes versus where the particles distribute. This study demonstrates the importance of developing particle systems that can use quantitative or even secondary measures to understand clearance and distribution."

5. Conclusions

In this study, a composite nanoparticle was developed to non-invasively visualize particle clearance via IVIS imaging and quantify particle biodistribution with selectivity and high sensitivity via EPR spectroscopy. After 14 days, EPR spectroscopy indicated greater nanoparticle retention in the 15-month old rats compared to the 5- and 10- month old rats, suggesting an age effect on clearance efficiency. Furthermore, EPR suggested more nanoparticles were retained in the OA knee compared to the contralateral knee, and 15-month animals had significantly more nanoparticle retention in both knees compared to the 5- and 10-month animals. While EPR provides a more accurate indication of particle

Author Manuscript Author Manuscript Author Manuscript Author Manuscript

distribution in each organ and joint tissue, IVIS can provide longitudinal data on particle clearance. Based on our results, both age and OA have an effect on nanoparticle distribution in the joint, and both factors should be considered when designing intra-articular drug delivery studies.

Supplementary Material

Refer to Web version on PubMed Central for supplementary material.

Acknowledgments

The authors thank Dr. Gail E. Fanucci for providing access to the EPR spectroscopy equipment. We thank Cory French and Andreina Chu for help with EPR spectroscopy data analysis. We also thank Kiara Chan, Yash Shah, Taylor Yeater, and Saumya Kapoor for assisting with sample processing.

Funding

This work was supported by the National Institutes of Health/ National Institute of Arthritis and Musculoskeletal and Skin Diseases [R01AR068424] and [R01AR071431]. Funding sources had no role in study design, data collection and analysis, manuscript preparation, or decision to publish.

References

[1]. Centers for Diesase Control, Osteoarthritis (OA), 2018. https://www.cdc.gov/arthritis/basics/osteoarthritis.htm.

[2]. Vos T, Flaxman AD, Naghavi M, Lozano R, Michaud C, Ezzati M, Shibuya K, Salomon JA, Abdalla S, Aboyans V, Abraham J, Ackerman I, Aggarwal R, Ahn SY, Ali MK, Alvarado M, Anderson HR, Anderson LM, Andrews KG, Atkinson C, Baddour LM, Bahalim AN, Barker-Collo S, Barrero LH, Bartels DH, Basáñez M-G, Baxter A, Bell ML, Benjamin EJ, Bennett D, Bernabé E, Bhalla K, Bhandari B, Bikbov B, Bin Abdulhak A, Birbeck G, Black JA, Blencowe H, Blore JD, Blyth F, Bolliger I, Bonaventure A, Boufous S, Bourne R, Boussinesq M, Braithwaite T, Brayne C, Bridgett L, Brooker S, Brooks P, Brugha TS, Bryan-Hancock C, Bucello C, Buchbinder R, Buckle G, Budke CM, Burch M, Burney P, Burstein R, Calabria B, Campbell B, Canter CE, Carabin H, Carapetis J, Carmona L, Cella C, Charlson F, Chen H, Cheng AT-A, Chou D, Chugh SS, Coffeng LE, Colan SD, Colquhoun S, Colson KE, Condon J, Connor MD, Cooper LT, Corriere M, Cortinovis M, de Vaccaro KC, Couser W, Cowie BC, Criqui MH, Cross M, Dabhadkar KC, Dahiya M, Dahodwala N, Damsere-Derry J, Danaei G, Davis A, De Leo D, Degenhardt L, Dellavalle R, Delossantos A, Denenberg J, Derrett S, Des Jarlais DC, Dharmaratne SD, Dherani M, Diaz-Torne C, Dolk H, Dorsey ER, Driscoll T, Duber H, Ebel B, Edmond K, Elbaz A, Ali SE, Erskine H, Erwin PJ, Espindola P, Ewoigbokhan SE, Farzadfar F, Feigin V, Felson DT, Ferrari A, Ferri CP, Fèvre EM, Finucane MM, Flaxman S, Flood L, Foreman K, Forouzanfar MH, Fowkes FGR, Franklin R, Fransen M, Freeman MK, Gabbe BJ, Gabriel SE, Gakidou E, Ganatra HA, Garcia B, Gaspari F, Gillum RF, Gmel G, Gosselin R, Grainger R, Groeger J, Guillemin F, Gunnell D, Gupta R, Haagsma J, Hagan H, Halasa YA, Hall W, Haring D, Haro JM, Harrison JE, Havmoeller R, Hay RJ, Higashi H, Hill C, Hoen B, Hoffman H, Hotez PJ, Hoy D, Huang JJ, Ibeanusi SE, Jacobsen KH, James SL, Jarvis D, Jasrasaria R, Jayaraman S, Johns N, Jonas JB, Karthikeyan G, Kassebaum N, Kawakami N, Keren A, Khoo J-P, King CH, Knowlton LM, Kobusingye O, Koranteng A, Krishnamurthi R, Lalloo R, Laslett LL, Lathlean T, Leasher JL, Lee YY, Leigh J, Lim SS, Limb E, Lin JK, Lipnick M, Lipshultz SE, Liu W, Loane M, Ohno SL, Lyons R, Ma J, Mabweijano J, MacIntyre MF, Malekzadeh R, Mallinger L, Manivannan S, Marcenes W, March L, Margolis DJ, Marks GB, Marks R, Matsumori A, Matzopoulos R, Mayosi BM, McAnulty JH, McDermott MM, McGill N, McGrath J, Medina-Mora ME, Meltzer M, Mensah GA, Merriman TR, Meyer A-C, Miglioli V, Miller M, Miller TR, Mitchell PB, Mocumbi AO, Moffitt TE, Mokdad AA, Monasta L, Montico M, Moradi-Lakeh M, Moran A, Morawska L, Mori R, Murdoch ME, Mwaniki MK, Naidoo K, Nair MN, Naldi L, Narayan KMV, Nelson PK, Nelson RG, Nevitt MC, Newton CR, Nolte S,

Author Manuscript Author Manuscript Author Manuscript Author Manuscript

Norman P, Norman R, O'Donnell M, O'Hanlon S, Olives C, Omer SB, Ortblad K, Osborne R, Ozgediz D, Page A, Pahari B, Pandian JD, Rivero AP, Patten SB, Pearce N, Padilla RP, Perez-Ruiz F, Perico N, Pesudovs K, Phillips D, Phillips MR, Pierce K, Pion S, V Polanczyk G, Polinder S, Pope CA, Popova S, Porrini E, Pourmalek F, Prince M, Pullan RL, Ramaiah KD, Ranganathan D, Razavi H, Regan M, Rehm JT, Rein DB, Remuzzi G, Richardson K, Rivara FP, Roberts T, Robinson C, De Leòn FR, Ronfani L, Room R, Rosenfeld LC, Rushton L, Sacco RL, Saha S, Sampson U, Sanchez-Riera L, Sanman E, Schwebel DC, Scott JG, Segui-Gomez M, Shahraz S, Shepard DS, Shin H, Shivakoti R, Singh D, Singh GM, Singh JA, Singleton J, Sleet DA, Sliwa K, Smith E, Smith JL, Stapelberg NJC, Steer A, Steiner T, Stolk WA, Stovner LJ, Sudfeld C, Syed S, Tamburlini G, Tavakkoli M, Taylor HR, Taylor JA, Taylor WJ, Thomas B, Thomson WM, Thurston GD, Tleyjeh IM, Tonelli M, Towbin JA, Truelsen T, Tsilimbaris MK, Ubeda C, Undurraga EA, van der Werf MJ, van Os J, Vavilala MS, Venketasubramanian N, Wang M, Wang W, Watt K, Weatherall DJ, Weinstock MA, Weintraub R, Weisskopf MG, Weissman MM, White RA, Whiteford H, Wiersma ST, Wilkinson JD, Williams HC, Williams SRM, Witt E, Wolfe F, Woolf AD, Wulf S, Yeh P-H, Zaidi AKM, Zheng Z-J, Zonies D, Lopez AD, Murray CJL, AlMazroa MA, Memish ZA, Murray CJ, Years lived with disability (YLDs) for 1160 sequelae of 289 diseases and injuries 1990–2010: a systematic analysis for the Global Burden of Disease Study 2010., Lancet (London, England). 380 (2012) 2163–96. doi:10.1016/S0140-6736(12)61729-2.

[3]. Hootman JM, Helmick CG, Barbour KE, Theis KA, Boring MA, Updated Projected Prevalence of Self-Reported Doctor-Diagnosed Arthritis and Arthritis-Attributable Activity Limitation Among US Adults, 2015–2040., Arthritis Rheumatol. (Hoboken, N.J.). 68 (2016) 1582–7. doi:10.1002/art.39692.

[4]. Zhang W, Moskowitz RW, Nuki G, Abramson S, Altman RD, Arden N, Bierma-Zeinstra S, Brandt KD, Croft P, Doherty M, Dougados M, Hochberg M, Hunter DJ, Kwoh K, Lohmander LS, Tugwell P, OARSI recommendations for the management of hip and knee osteoarthritis, Part II: OARSI evidence-based, expert consensus guidelines, Osteoarthritis and Cartilage. 16 (2008) 137–162. doi:10.1016/j.joca.2007.12.013. [PubMed: 18279766]

[5]. Evans CH, Kraus VB, Setton LA, Progress in intra-articular therapy., Nat. Rev. Rheumatol. 10 (2014) 11–22. doi:10.1038/nrrheum.2013.159. [PubMed: 24189839]

[6]. Gouveia VM, Lima SAC, Nunes C, Reis S, Non-biologic nanodelivery therapies for rheumatoid arthritis, J. Biomed. Nanotechnol. 11 (2015) 1701–1721. doi:10.1166/jbn.2015.2159. [PubMed: 26502635]

[7]. Brown S, Kumar S, Sharma B, Intra-articular targeting of nanomaterials for the treatment of osteoarthritis, Acta Biomater. (2019). doi:10.1016/j.actbio.2019.03.010.

[8]. Mwangi T, Setton LA, Adams SB, Chen J, Guilak F, Yuan F, The Intra-Articular Clearance of Silk Microparticles and Macromolecules in Healthy and Arthritic Rat Knee Joints, Duke University, 2015. https://dukespace.lib.duke.edu/dspace/bitstream/handle/10161/11305/Mwangi_duke_0066D_13136.pdf?sequence=1&isAllowed=y (accessed April 23, 2018).

[9]. Whitmire RE, Wilson DS, Singh A, Levenston ME, Murthy N, García AJ, Self-assembling nanoparticles for intra-articular delivery of anti-inflammatory proteins., Biomaterials. 33 (2012) 7665–75. doi:10.1016/j.biomaterials.2012.06.101. [PubMed: 22818981]

[10]. Butoescu N, Seemayer CA, Palmer G, Guerne P-A, Gabay C, Doelker E, Jordan O, Magnetically retainable microparticles for drug delivery to the joint: efficacy studies in an antigen-induced arthritis model in mice., Arthritis Res. Ther. 11 (2009) R72. doi:10.1186/ar2701.

[11]. Pradal J, Maudens P, Gabay C, Seemayer CA, Jordan O, Allémann E, Effect of particle size on the biodistribution of nano- and microparticles following intra-articular injection in mice, Int. J. Pharm. 498 (2016) 119–129. doi:10.1016/J.IJPHARM.2015.12.015. [PubMed: 26685724]

[12]. Kim SR, Ho MJ, Lee E, Lee JW, Choi YW, Kang MJ, Cationic PLGA/Eudragit RL nanoparticles for increasing retention time in synovial cavity after intra-articular injection in knee joint., Int. J. Nanomed. 10 (2015) 5263–71. doi:10.2147/IJN.S88363.

[13]. Hootman JM, Helmick CG, Projections of US prevalence of arthritis and associated activity limitations, Arthritis Rheum. 54 (2006) 226–229. doi:10.1002/art.21562. [PubMed: 16385518]

[14]. Felson DT, Lawrence RC, Dieppe PA, Hirsch R, Helmick CG, Jordan JM, Kington RS, Lane NE, Nevitt MC, Zhang Y, Sowers M, McAlindon T, Spector TD, Poole AR, Yanovski SZ, Ateshian G,

Author Manuscript Author Manuscript Author Manuscript Author Manuscript

Sharma L, Buckwalter JA, Brandt KD, Fries JF, Osteoarthritis: New Insights. Part 1: The Disease and Its Risk Factors, Ann. Intern. Med. 133 (2000) 635. doi:10.7326/0003-4819-133-8-200010170-00016. [PubMed: 11033593]

[15]. Zolla V, Nizamutdinova IT, Scharf B, Clement CC, Maejima D, Akl T, Nagai T, Luciani P, Leroux J-C, Halin C, Stukes S, Tiwari S, Casadevall A, Jacobs WR, Entenberg D, Zawieja DC, Condeelis J, Fooksman DR, Gashev AA, Santambrogio L, Aging-related anatomical and biochemical changes in lymphatic collectors impair lymph transport, fluid homeostasis, and pathogen clearance, Aging Cell. 14 (2015) 582–594. https://www.ncbi.nlm.nih.gov/pmc/articles/PMC4531072/pdf/acel0014-0582.pdf (accessed April 11, 2018). [PubMed: 25982749]

[16]. Kushner I, Somerville JA, Permeability of Human Synovial Membrane to Plasma Proteins Relationship to Molecular Size and Inflammation, Arthritis Rheum. (1969). https://onlinelibrary.wiley.com/doi/pdf/10.1002/art.1780140503 (accessed April 4, 2018).

[17]. Pasquali-Ronchetti I, Frizziero L, Guerra D, Baccarani-Contri M, Focherini MC, Georgountzos A, Vin-cenzi D, Cicchetti F, Perbellini A, Govoni E, Aging of the human synovium: An in vivo and ex vivo morphological study, Semin. Arthritis Rheum. 21 (1992) 400–414. doi:10.1016/0049-0172(92)90041-B.

[18]. Betre H, Liu W, Zalutsky MR, Chilkoti A, Kraus VB, Setton LA, A thermally responsive biopolymer for intra-articular drug delivery, J. Control. Release. 115 (2006) 175–182. doi:10.1016/J.JCONREL.2006.07.022. [PubMed: 16959360]

[19]. Owen SG, Francis HW, Roberts MS, Disappearance kinetics of solutes from synovial fluid after intra-articular injection., Br. J. Clin. Pharmacol. 38 (1994) 349–55. http://www.ncbi.nlm.nih.gov/pubmed/7833225 (accessed November 8, 2018). [PubMed: 7833225]

[20]. Larsen NE, Dursema HD, Pollak CT, Skrabut EM, Clearance kinetics of a hylan-based viscosupplement after intra-articular and intravenous administration in animal models, J. Biomed. Mater. Res. Part B Appl. Biomater. 100B (2012) 457–462. doi:10.1002/jbm.b.31971.

[21]. Thakkar H, Sharma RK, Mishra AK, Chuttani K, Murthy RSR, Celecoxib Incorporated Chitosan Microspheres: In Vitro and In Vivo Evaluation, J. Drug Target. 12 (2004) 549–557. doi:10.1080/10611860400010630. [PubMed: 15621680]

[22]. Edwards SHR, Cake MA, Spoelstra G, Read RA, Biodistribution and Clearance of Intra-articular Liposomes in a Large Animal Model Using a Radiographic Marker, J. Liposome Res. 17 (2007) 0–0. doi:10.1080/08982100701557129.

[23]. Cho H, Magid R, Danila DC, Hunsaker T, Pinkhassik E, Hasty KA, Theranostic Immunoliposomes for Osteoarthritis HHS Public Access, Nanomedicine. 10 (2016) 619–627. https://www.ncbi.nlm.nih.gov/pmc/articles/PMC4962614/pdf/nihms530171.pdf (accessed November 14, 2018).

[24]. Wahajuddin S. Arora, Superparamagnetic iron oxide nanoparticles: Magnetic nanoplatforms as drug carriers, Int. J. Nanomed. 7 (2012) 3445–3471. doi:10.2147/IJN.S30320.

[25]. Ding H, Wu F, Image guided biodistribution and pharmacokinetic studies of theranostics, Theranostics. 2 (2012) 1040–1053. doi:10.7150/thno.4652. [PubMed: 23227121]

[26]. Liu Y, Tseng Y-C, Huang L, Biodistribution studies of nanoparticles using fluorescence imaging: a qualitative or quantitative method?, Pharm. Res. 29 (2012) 3273–7. doi:10.1007/s11095-012-0818-1. [PubMed: 22806405]

[27]. Chertok B, Cole AJ, David AE, Yang VC, Comparison of Electron Spin Resonance Spectroscopy and Inductively-Coupled Plasma Optical Emission Spectroscopy for Biodistribution Analysis of Iron-Oxide Nanoparticles, Mol. Pharm. 7 (2009) 375–385. https://pubs.acs.org/doi/10.1021/mp900161h. (accessed June 3, 2019).

[28]. Danhier P, De Preter G, Magat J, Godechal Q, Porporato PE, Jordan BF, Feron O, Sonveaux P, Gallez B, Multimodal cell tracking of a spontaneous metastasis model: comparison between MRI, electron paramagnetic resonance and bioluminescence, Contrast Media Mol. Imaging. 9 (2014) 143–153. doi:10.1002/cmmi.1553. [PubMed: 24523059]

[29]. Gobbo OL, Wetterling F, Vaes P, Teughels S, Markos F, Edge D, Shortt CM, Crosbie-Staunton K, Radomski MW, Volkov Y, Prina-Mello A, Biodistribution and pharmacokinetic studies of SPION using particle electron paramagnetic resonance, MRI and ICP-MS, Nanomedicine. 10 (2015) 1751–1760. doi:10.2217/nnm.15.22. [PubMed: 26080697]

Author Manuscript Author Manuscript Author Manuscript Author Manuscript

[30]. Chertok B, Moffat BA, David AE, Yu F, Bergemann C, Ross BD, Yang VC, Iron Oxide Nanoparticles as a Drug Delivery Vehicle for MRI Monitored Magnetic Targeting of Brain Tumors, Biomaterials. 29 (2008) 487. doi:10.1016/J.BIOMATERIALS.2007.08.050. [PubMed: 17964647]

[31]. Unni M, Uhl AM, Savliwala S, Savitzky BH, Dhavalikar R, Garraud N, Arnold DP, Kourkoutis LF, Andrew JS, Rinaldi C, Thermal Decomposition Synthesis of Iron Oxide Nanoparticles with Diminished Magnetic Dead Layer by Controlled Addition of Oxygen, ACS Nano. 11 (2017) 2284–2303. https://pubs.acs.org/doi/pdf/10.1021/acsnano.7b00609 (accessed April 3, 2018). [PubMed: 28178419]

[32]. Pinkerton NM, Gindy ME, Calero-DdelC VL, Wolfson T, Pagels RF, Adler D, Gao D, Li S, Wang R, Zevon M, Yao N, Pacheco C, Therien MJ, Rinaldi C, Sinko PJ, Prud'homme RK, Single-Step Assembly of Multimodal Imaging Nanocarriers: MRI and Long-Wavelength Fluorescence Imaging., Adv. Healthc. Mater. 4 (2015) 1376–85. doi:10.1002/adhm.201400766. [PubMed: 25925128]

[33]. Abràmoff MD, Magalhaes PJ, Ram SJ, Image Processing with ImageJ, Biophotonics Int. 11 (2004) 36–42. https://imagescience.org/meijering/publications/download/bio2004.pdf (accessed July 19, 2019).

[34]. Chantrell R, Popplewell J, Charles S, Measurements of particle size distribution parameters in ferrofluids, IEEE Trans. Magn. 14 (1978) 975–977. doi:10.1109/TMAG.1978.1059918.

[35]. Fannin PC, Investigating magnetic fluids by means of complex susceptibility measurements, J. Magn. Magn. Mater. 258–259 (2003) 446–451. https://www.sciencedirect.com/science/article/pii/S0304885302010934 (accessed July 21, 2019).

[36]. Shliomis MI, Stepanov VI, Theory of the Dynamic Susceptibility of Magnetic Fluids, in: Relax. Phenom. Condens. Matter, John Wiley & Sons, Ltd, 1994: pp. 1–30. http://doi.wiley.com/10.1002/9780470141465.ch1 (accessed July 21, 2019).

[37]. Kang ML, Ko J-Y, Kim JE, Im G-I, Intra-articular delivery of kartogenin-conjugated chitosan nano/microparticles for cartilage regeneration, Biomaterials. 35 (2014) 9984–9994. doi:10.1016/J.BIOMATERIALS.2014.08.042. [PubMed: 25241157]

[38]. Seifer DR, Furman BD, Guilak F, Olson SA, Brooks SC, Kraus VB, Novel synovial fluid recovery method allows for quantification of a marker of arthritis in mice, Osteoarthritis and Cartilage. 16 (2008) 1532–1538. https://www.ncbi.nlm.nih.gov/pmc/articles/PMC2602808/pdf/nihms80866.pdf (accessed May 7, 2019). [PubMed: 18538588]

[39]. Sacchetti C, Liu-Bryan R, Magrini A, Rosato N, Bottini N, Bottini M, Polyethylene-Glycol-Modified Single-Walled Carbon Nanotubes for Intra-Articular Delivery to Chondrocytes, ACS Nano. 8 (2014) 12280–12291. www.acsnano.org12280 (accessed July 16, 2019). [PubMed: 25415768]

[40]. Singh PA, Agarwal DR, Diaz-Ruiz CA, Willett DNJ, Wang P, Lee DLA, Wang PQ, Guldberg PRE, García PAJ, Nano-engineered particles for enhanced intra-articular retention and delivery of proteins, Adv. Healthc. Mater. 3 (2014) 1562. doi:10.1002/ADHM.201400051. [PubMed: 24687997]

[41]. Kang M-L, Kim J-E, Im G-I, Thermoresponsive nanospheres with independent dual drug release profiles for the treatment of osteoarthritis, Acta Biomater. 39 (2016) 65–78. doi:10.1016/J.ACTBIO.2016.05.005. [PubMed: 27155347]

[42]. Bajpayee AG, Scheu M, Grodzinsky AJ, Porter RM, Electrostatic interactions enable rapid penetration, enhanced uptake and retention of intra-articular injected avidin in rat knee joints, J. Orthop. Res. 32 (2014) 1044–1051. doi:10.1002/jor.22630. [PubMed: 24753019]

[43]. Geiger BC, Wang S, Padera RF, Grodzinsky AJ, Hammond PT, Cartilage-penetrating nanocarriers improve delivery and efficacy of growth factor treatment of osteoarthritis, Sci. Transl. Med. 10 (2018) eaat8800. doi:10.1126/SCITRANSLMED.AAT8800.

[44]. Morgen M, Tung D, Boras B, Miller W, Malfait A-M, Tortorella M, Nanoparticles for Improved Local Retention after Intra-Articular Injection into the Knee Joint, Pharm. Res. 30 (2013) 257–268. doi:10.1007/s11095-012-0870-x. [PubMed: 22996566]

[45]. Hu H-Y, Lim N-H, Ding-Pfennigdorff D, Saas J, Wendt KU, Ritzeler O, Nagase H, Plettenburg O, Schultz C, Nazare M, DOTAM Derivatives as Active Cartilage-Targeting Drug Carriers for the

Author Manuscript Author Manuscript Author Manuscript Author Manuscript

Treatment of Osteoarthritis, Bioconjug. Chem. 26 (2015) 383–388. doi:10.1021/bc500557s. [PubMed: 25629889]

[46]. Mwangi TK, Berke IM, Nieves EH, Bell RD, Adams SB, Setton LA, Intra-articular clearance of labeled dextrans from naive and arthritic rat knee joints, J. Control. Release. 283 (2018) 76–83. doi:10.1016/J.JCONREL.2018.05.029. [PubMed: 29842918]

[47]. Cole AJ, David AE, Wang J, Galbán CJ, Yang VC, Magnetic brain tumor targeting and biodistribution of long-circulating PEG-modified, cross-linked starch-coated iron oxide nanoparticles, Biomaterials. 32 (2011) 6291–6301. doi:10.1016/J.BIOMATERIALS.2011.05.024. [PubMed: 21684593]

[48]. Mangoni AA, Jackson SHD, Age-related changes in pharmacokinetics and pharmacodynamics: basic principles and practical applications., Br. J. Clin. Pharmacol. 57 (2004) 6–14. doi:10.1046/j.1365-2125.2003.02007.x. [PubMed: 14678335]

[49]. Le Couteur D, Cogger VC, Markus AMA, Harvey PJ, Yin Z, Ansselin AD, McLean AJ, Pseudocapillarization and associated energy limitation in the aged rat liver, Hepatology. 33 (2001) 537–543. doi:10.1053/jhep.2001.22754. [PubMed: 11230732]

[50]. Doan TN, Bernard FC, McKinney JM, Dixon JB, Willett NJ, Endothelin-1 inhibits size dependent lymphatic clearance of PEG-based conjugates after intra-articular injection into the rat knee, Acta Biomater. 93 (2019) 270–281. https://www.sciencedirect.com/science/article/pii/S1742706119302661?via%3Dihub (accessed May 30, 2019). [PubMed: 30986528]

[51]. Moore JE, Bertram CD, Bertram CD, Lymphatic System Flows., Annu. Rev. Fluid Mech. 50 (2018) 459–482. doi:10.1146/annurev-fluid-122316-045259. [PubMed: 29713107]

[52]. Shi J, Liang Q, Zuscik M, Shen J, Chen D, Xu H, Wang Y-J, Chen Y, Wood RW, Li J, Boyce BF, Xing L, Distribution and alteration of lymphatic vessels in knee joints of normal and osteoarthritic mice., Arthritis Rheumatol. (Hoboken, N.J.). 66 (2014) 657–66. doi:10.1002/art.38278.

[53]. Singh A, Agarwal R, Diaz-Ruiz CA, Willett NJ, Wang P, Lee LA, Wang Q, Guldberg RE, García AJ, Nanoengineered Particles for Enhanced Intra-Articular Retention and Delivery of Proteins, Adv. Healthc. Mater. 3 (2014) 1562–1567. doi:10.1002/adhm.201400051. [PubMed: 24687997]

[54]. Fuller EG, Scheutz GM, Jimenez A, Lewis P, Liu S, Sumerlin BS, Rinaldi C, Theranostic Nanocarriers Combining High Drug Loading and Magnetic Particle Imaging, Int. J. Pharm. (2019) 118796. doi:10.1016/j.ijpharm.2019.118796. [PubMed: 31678389]

[55]. Danhier P, Gallez B, Electron paramagnetic resonance: A powerful tool to support magnetic resonance imaging research, Contrast Media Mol. Imaging. 10 (2015) 266–281. doi:10.1002/cmmi.1630. [PubMed: 25362845]

[56]. Vangijzegem T, Stanicki D, Laurent S, Magnetic iron oxide nanoparticles for drug delivery: applications and characteristics, Expert Opin. Drug Deliv. 16 (2019) 69–78. doi:10.1080/17425247.2019.1554647. [PubMed: 30496697]

[57]. Monnier CA, Burnand D, Rothen-Rutishauser B, Lattuada M, Petri-Fink A, Magnetoliposomes: Opportunities and challenges, Eur. J. Nanomedicine. 6 (2014) 201–215. doi:10.1515/ejnm-2014-0042.

[58]. Wijaya A, Hamad-Schifferli K, High-density encapsulation of Fe3O4 nanoparticles in lipid vesicles, Langmuir. 23 (2007) 9546–9550. doi:10.1021/la701128b. [PubMed: 17696555]

[59]. Rothenfluh DA, Bermudez H, O'Neil CP, Hubbell JA, Biofunctional polymer nanoparticles for intra-articular targeting and retention in cartilage, Nat. Mater. 7 (2008) 248–254. doi:10.1038/nmat2116. [PubMed: 18246072]

[60]. Brown S, Pistiner J, Adjei IM, Sharma B, Nanoparticle Properties for Delivery to Cartilage: The Implications of Disease State, Synovial Fluid, and Off-Target Uptake, Mol. Pharm. 16 (2019) 469–479. doi:10.1021/acs.molpharmaceut.7b00484. [PubMed: 28669194]

[61]. Mwangi TK, Bowles RD, Tainter DM, Bell RD, Kaplan DL, Setton LA, Synthesis and characterization of silk fibroin microparticles for intra-articular drug delivery, Int. J. Pharm. 485 (2015) 7–14. doi:10.1016/J.IJPHARM.2015.02.059. [PubMed: 25724134]

Author Manuscript Author Manuscript Author Manuscript Author Manuscript

- Electron paramagnetic resonance spectroscopy can sensitively assess biodistribution
- Particles clear more slowly from OA knees compared to contralateral controls
- Intra-articular particle retention is increased in older animals

Author Manuscript Author Manuscript Author Manuscript Author Manuscript

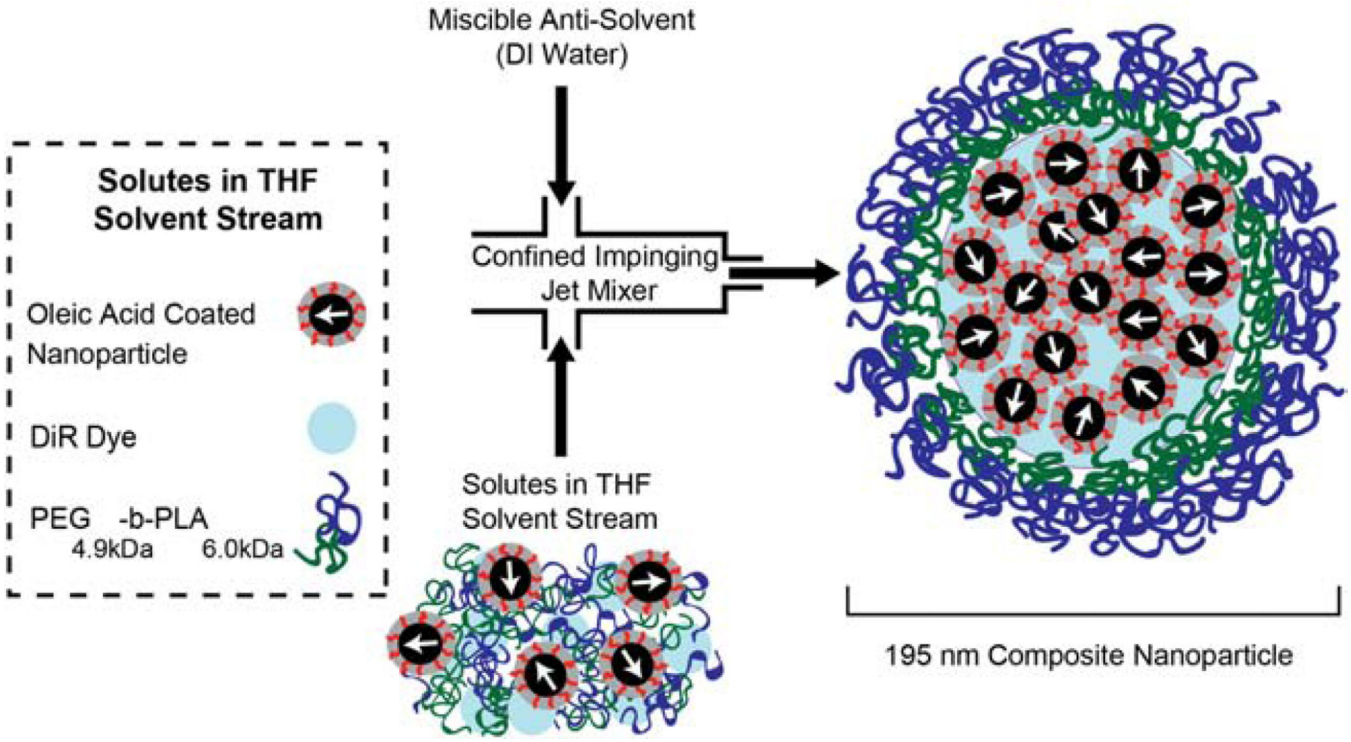

Fig. 1: Flash nanoprecipitation was used to create composite nanoparticles.

First, oleic acid coated nanoparticles (58 wt%), DiR dye (6 wt%), and $PEG_{4.9kDa}$-b-$PLA_{6.0kDa}$ (36 wt%) were suspended in tetrahydrofuran (THF). Then, solutes and THF were rapidly mixed with DI water in a confined impinging jet mixer. (2-column fitting image)

Author Manuscript
Author Manuscript
Author Manuscript
Author Manuscript

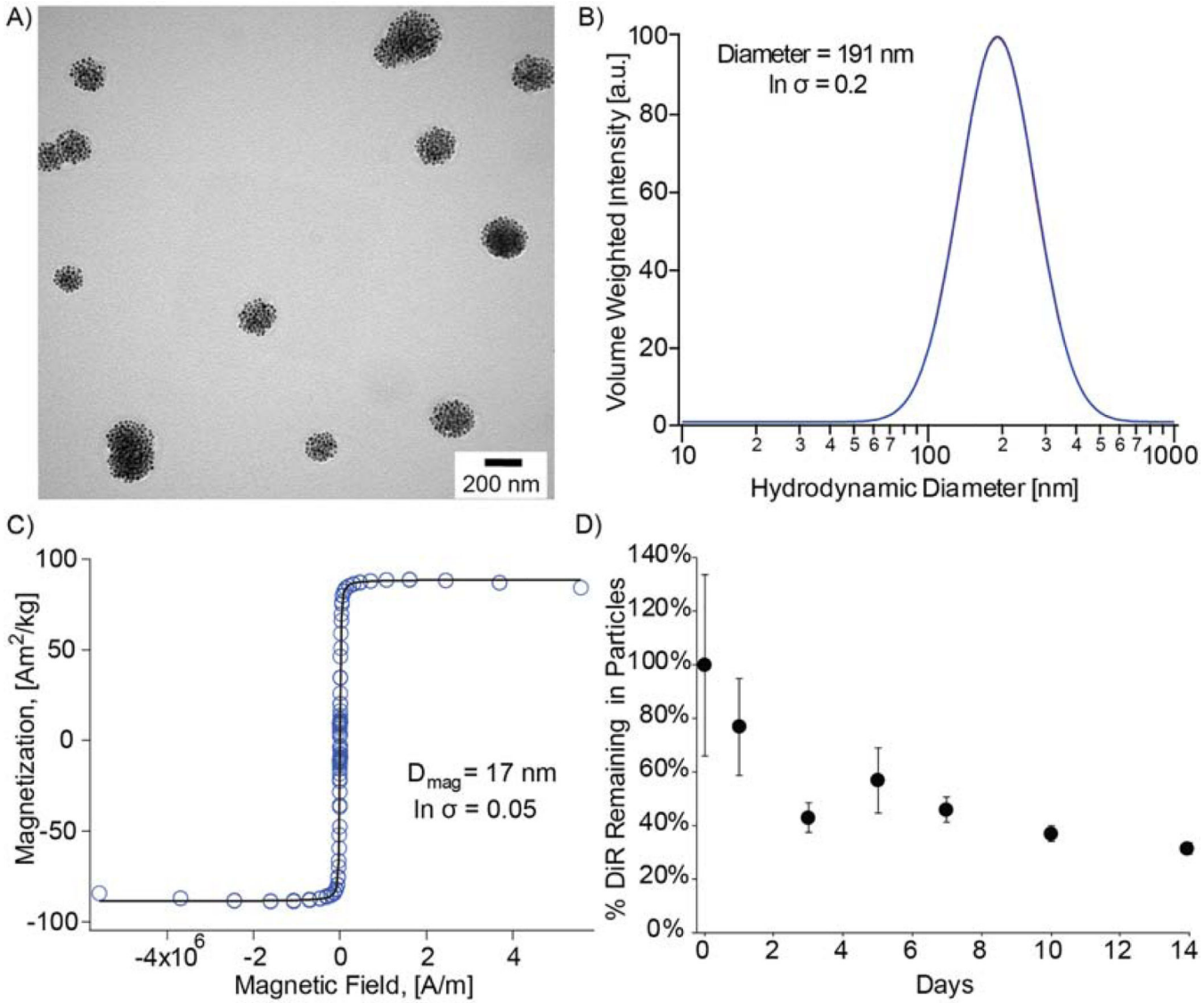

Fig. 2: Composite nanoparticle characterization.

A) TEM images of 200 nm physical diameter composite nanoparticles. B) Volume-weighted median diameter obtained from the DLS log-normal distribution for 191 nm hydrodynamic diameter composite nanoparticles. C) Equilibrium magnetization curve for iron oxide nanoparticles with a 17 nm magnetic diameter and 86 Am^2/kg saturation magnetization. D) DiR stability in magnetic nanoparticles incubated in synovial fluid over 14 days. (2-column fitting image)

Author Manuscript Author Manuscript Author Manuscript Author Manuscript

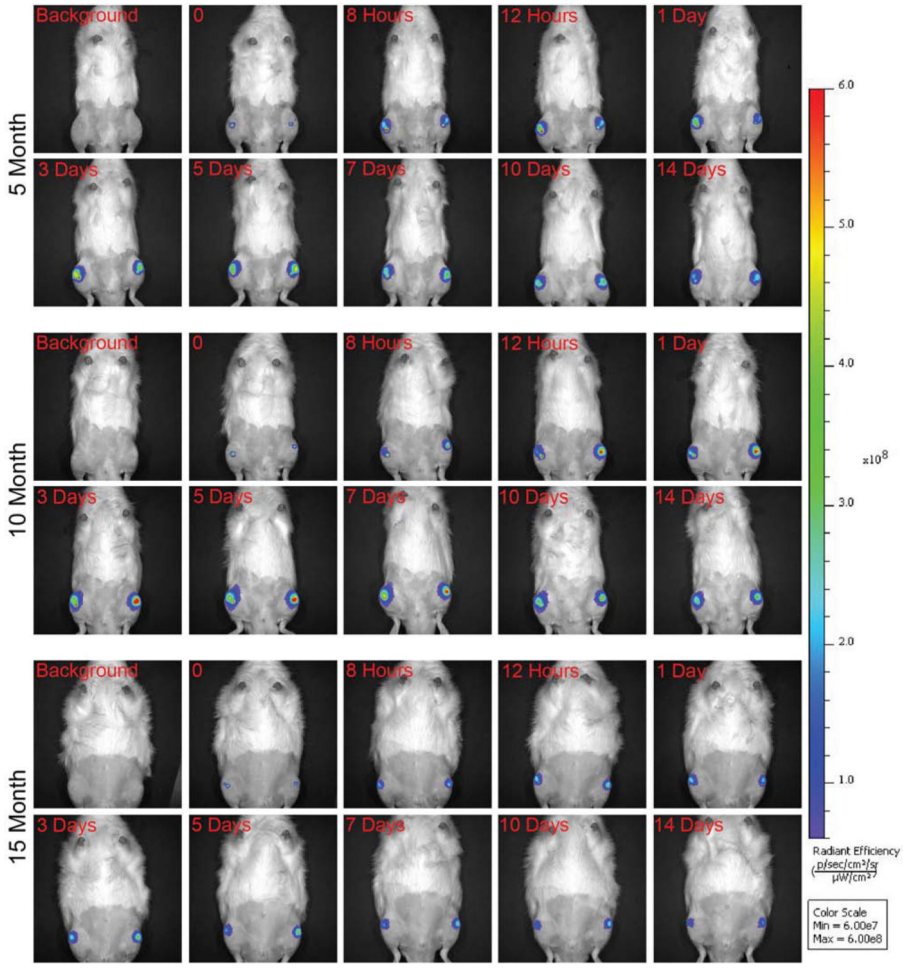

Fig. 3: Representative IVIS images of 5-, 10-, and 15-month rats over the course of 14 days.
Background IVIS images were taken prior to injection. Then, rats were injected with composite nanoparticles and immediately imaged (represented in the time 0 images). Rats were then imaged at various time points over the course of 14 days (2-column fitting image).

Author Manuscript Author Manuscript Author Manuscript Author Manuscript

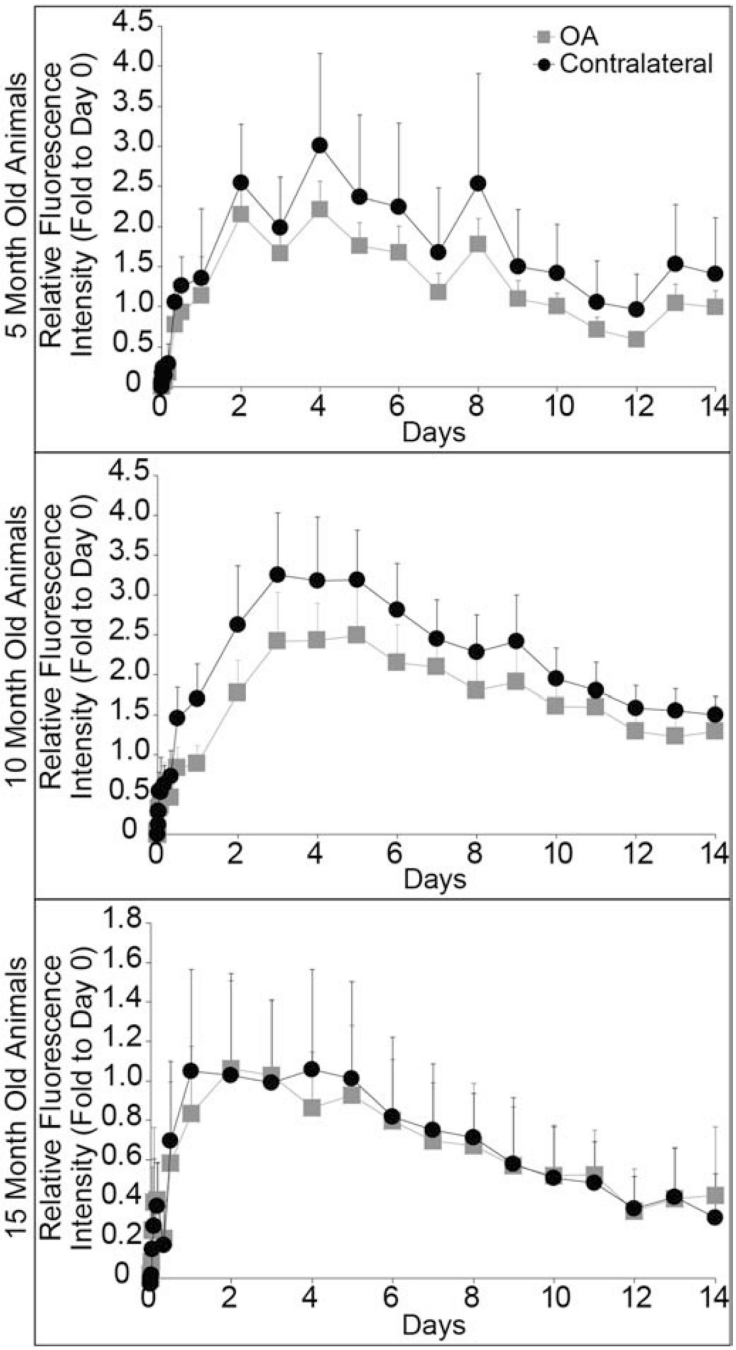

Fig. 4: *In vivo* composite nanoparticle clearance from OA and contralateral knees determined using IVIS.

There were no differences between nanoparticle clearance from the OA and contralateral joints for 5-month ($p = 0.2$) and 15-month rats ($p = 0.8$). OA and contralateral joint clearance was significantly different for 10-month rats ($p = 0.03$). All data were normalized by individual rat to its day 0 radiant efficiency value, and presented as mean + 95% confidence intervals. (Single column fitting image)

Author Manuscript Author Manuscript Author Manuscript Author Manuscript

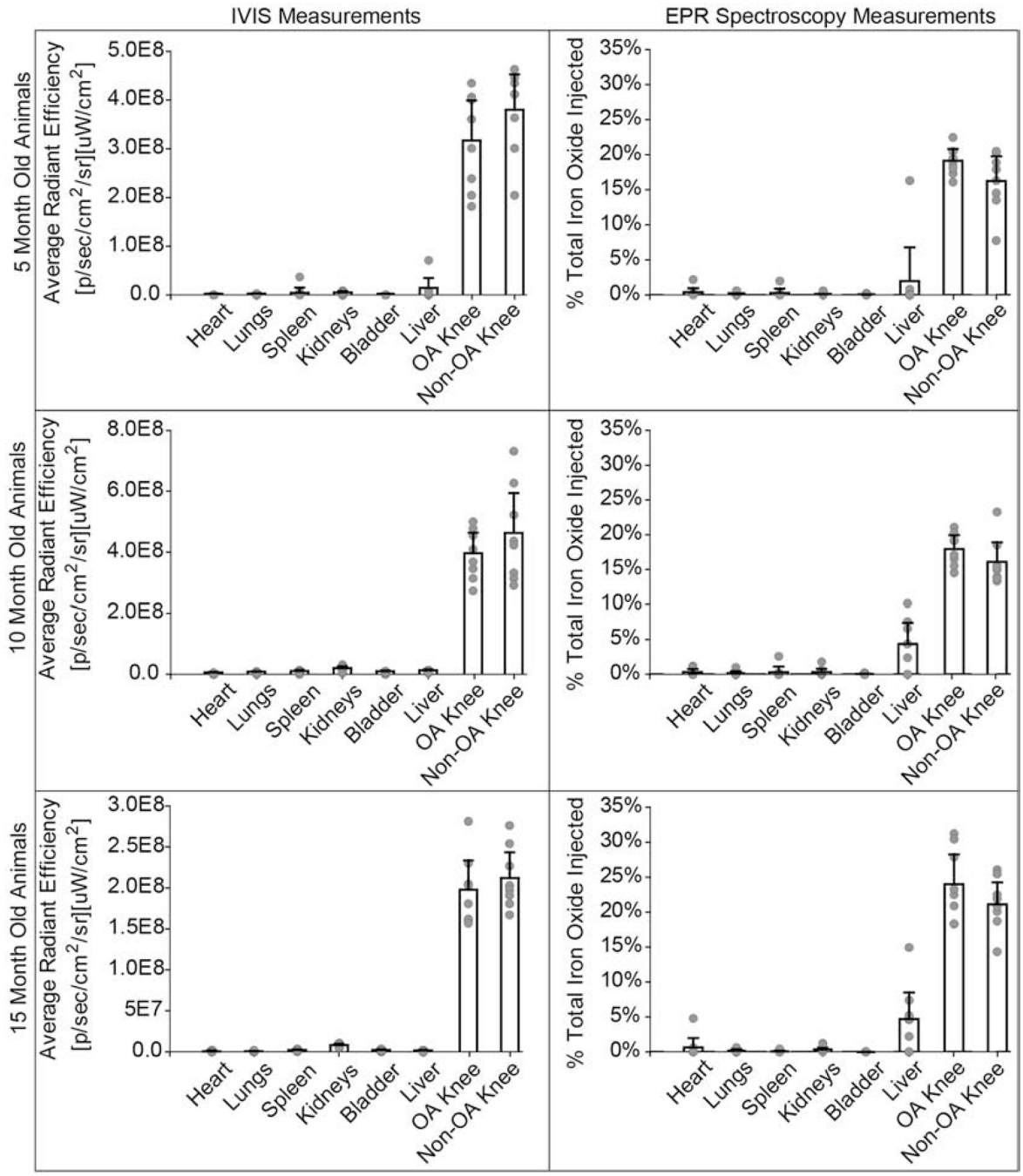

Fig. 5: IVIS and EPR spectroscopy comparison for composite nanoparticle biodistribution in vital organs.

Both IVIS and EPR show a predominant signal in the OA and contralateral knee. EPR shows nanoparticle accumulation in the liver for the 10- and 15-month rats, whereas IVIS does not show liver signal for 10- and 15-month rats. The dashed line represents the EPR lower limit of detection = 0.066 μg iron or 0.057% of total iron injected. Bar graphs represent mean + 95% confidence interval. (2-column fitting image)

Author Manuscript
Author Manuscript
Author Manuscript
Author Manuscript

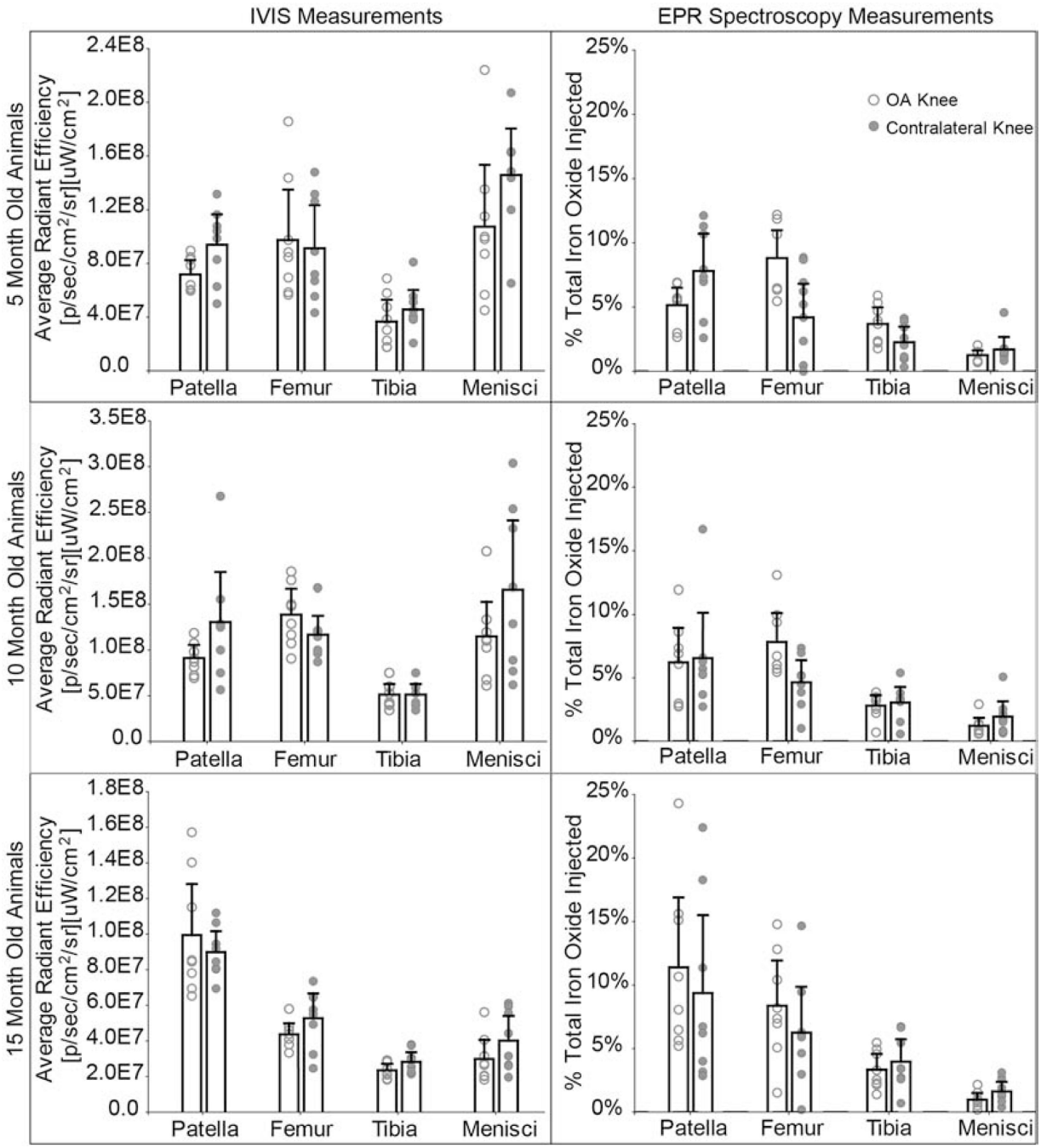

Fig. 6: IVIS and EPR spectroscopy comparison for composite nanoparticle distribution in knee tissues.

IVIS and EPR show nanoparticle accumulation in the tissues of the knee. IVIS illustrates greater nanoparticle accumulation in the menisci in the 5- and 10-month animals, while EPR indicates the least amount of nanoparticle accumulation in the menisci for all ages. EPR suggests a large fraction of composite nanoparticles distribute to the patellar tissue. The dashed line represents the EPR lower limit of detection = 0.066 μg iron or 0.057% of total iron injected. Bar graphs represent mean + 95% confidence interval. (2-column fitting image)

Author Manuscript Author Manuscript Author Manuscript Author Manuscript

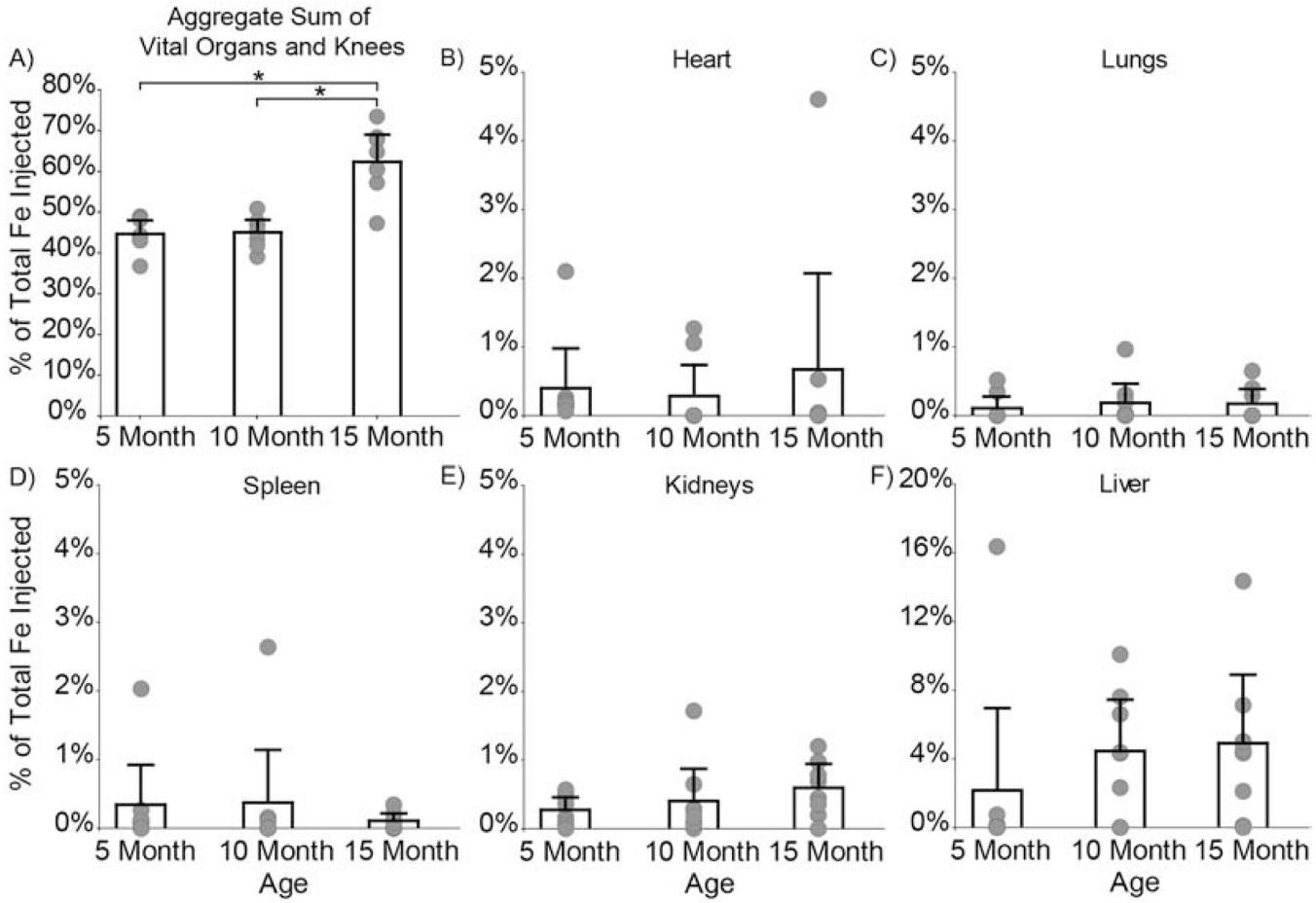

Fig. 7: Composite nanoparticle distribution in the body and vital organs quantified using EPR spectroscopy.

A) After 14 days, 44.7% of composite nanoparticles remained in the 5-month rats, 45.1% remained in the 10-month rats, and 62.5% remained in the 15-month rats. Significantly more nanoparticles remained in the 15-month compared to the 5- ($p = 0.0002$) and 10-month ($p = 0.0002$) rats. Nanoparticle distribution in the whole body was further analyzed to determine nanoparticle accumulation in the B) heart, C) lungs, D) spleen, E) kidneys, and F) liver. No differences were found for particle distribution in vital organs as a function of age. Bar graphs represent mean + 95% confidence interval. (2-column fitting image)

Author Manuscript Author Manuscript Author Manuscript Author Manuscript

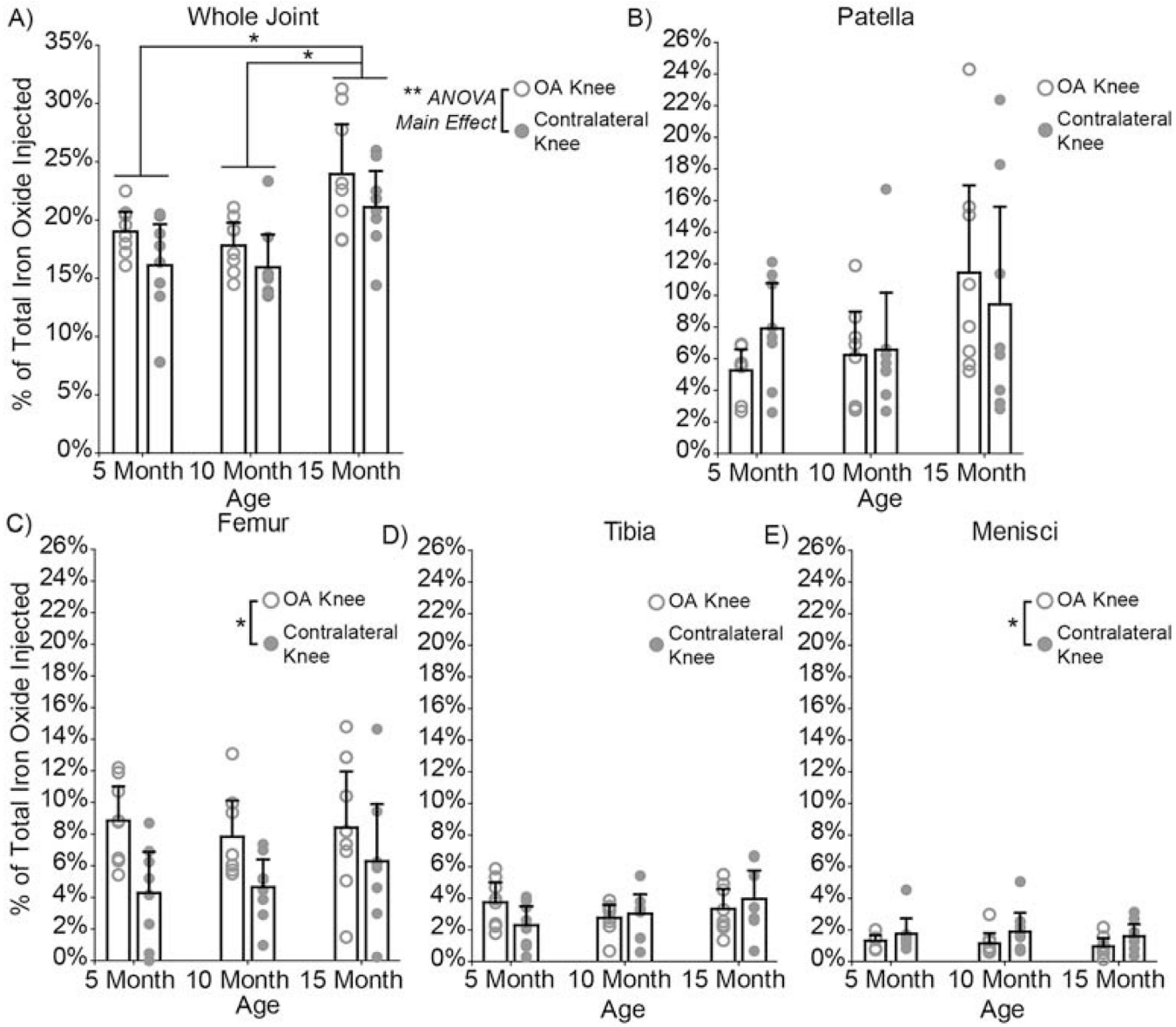

Fig. 8: Composite nanoparticle distribution in OA and contralateral knees and joint tissue regions quantified using EPR spectroscopy.

A) After 14 days, 15-month rats had significantly more nanoparticles in their knees than the 5-month ($p = 0.002$) and 10-month ($p = 0.0004$) rats. The 15-month rats had a total of 45.3% of the particles retained in their knees, whereas the 5- and 10-month rats had 35.3% and 34.0% respectively. Significant differences were found in nanoparticle distribution in OA and contralateral knees ($p = 0.02$, ANOVA, main effect), with more nanoparticles remaining in the OA knee. Nanoparticle distribution in the whole joint was further analyzed to determine nanoparticle accumulation in each tissue region. Most nanoparticles distributed to the patella/fat pad region B), followed by the femoral tissue region C), the tibial tissue region D), and lastly the menisci E). Age was a significant factor for nanoparticle accumulation in the patella/fat pad region ($p = 0.04$, ANOVA, main effect). Whereas, disease played a significant role in particle accumulation in the femoral tissue ($p = 0.002$) and the

menisci ($p = 0.04$). No differences were found for the tibial tissue region. Bar graphs represent mean + 95% confidence interval. (2-column fitting image)

Author Manuscript Author Manuscript Author Manuscript Author Manuscript